J. metamorphic Geol., 2004, **22,** 249–264 doi:10.1111/j.1525-1314.2004.00511.x

The pressure–temperature–time path of migmatites from the Sikkim Himalaya

N. B. W. HARRIS,[1] M. CADDICK,[2] J. KOSLER,[3] S. GOSWAMI,[2] D. VANCE[4] AND A. G. TINDLE[1]
[1]*Department of Earth Sciences, Open University, Milton Keynes, MK7 6AA UK (n.b.w.harris@open.ac.uk)*
[2]*Department of Earth Sciences, University of Cambridge, Cambridge CB2 3EQ, UK*
[3]*Department of Geochemistry, Charles University, Albertov 6, Prague 2, CZ-128 43, Czech Republic*
[4]*Department of Earth Sciences, University of Bristol, Wills Memorial Building, Bristol, BS8 1RJ, UK*

ABSTRACT A combined metamorphic and isotopic study of lit-par-lit migmatites exposed in the hanging wall of the Main Central Thrust (MCT) from Sikkim has provided a unique insight into the pressure–temperature–time path of the High Himalayan Crystalline Series of the eastern Himalaya. The petrology and geochemistry of one such migmatite indicates that the leucosome comprises a crystallized peraluminous granite coexisting with sillimanite and alkali feldspar. Large garnet crystals (2–3 mm across) are strongly zoned and grew initially within the kyanite stability field. The melanosome is a biotite–garnet pelitic gneiss, with fibrolitic sillimanite resulting from polymorphic inversion of kyanite. By combining garnet zoning profiles with the NaCaMnKFMASHTO pseudosection appropriate to the bulk composition of a migmatite retrieved from *c*. 1 km above the thrust zone, it has been established that early garnet formed at pressures of 10–12 kbar, and that subsequent decompression caused the rock to enter the melt field at *c*. 8 kbar and *c*. 750 °C, generating peritectic sillimanite and alkali feldspar by the incongruent melting of muscovite. Continuing exhumation resulted in resorption of garnet. Sm–Nd growth ages of garnet cores and rim, indicate pre-decompression garnet growth at 23 ± 3 Ma and near-peak temperatures during melting at 16 ± 2 Ma. This provides a decompression rate of 2 ± 1 mm yr^{-1} that is consistent with exhumation rates inferred from mineral cooling ages from the eastern Himalaya. Simple 1D thermal modelling confirms that exhumation at this rate would result in a near-isothermal decompression path, a result that is supported by the phase relations in both the melanosome and leucosome components of the migmatite. Results from this study suggest that anatexis of Miocene granite protoliths from the Himalaya was a consequence of rapid decompression, probably in response to movement on the MCT and on the South Tibetan detachment to the north.

Key words: garnet zoning; migmatite; pseudosection; Sikkim Himalaya; Sm–Nd dating.

INTRODUCTION

Understanding the tectonic evolution of a collision zone requires a precise knowledge of the *P–T–t* path of exposed rocks that are deformed and metamorphosed by the orogeny. In particular, the timing and location of melting during orogenesis underpins our understanding of the rheological behaviour of tectonically thickened crust. This problem is usually tackled by combining thermobarometry, obtained from coexisting phases assumed to be in equilibrium, with isotopic constraints that rely on U–Pb accessory phase chronometry. However, the dating of an accessory phase is only of use for understanding the chronology of deformation or metamorphic events if the growth of that phase can be related to the growth of fabric-forming and *P–T* sensitive phases (Harrison *et al.*, 1997; Foster *et al.*, 2000). For this study we have combined thermobarometry and *P–T* paths deduced from pseudosection analysis with precise isotope dating of garnet, a fabric-forming and *P–T* sensitive phase. This approach has been attempted before for a few Himalayan assemblages using either direct Sm–Nd dating of garnet or dating of accessory phases with a clear textural relationship with garnet growth (Vance & Harris, 1999; Foster *et al.*, 2002) but hitherto these studies have been restricted to sub-solidus assemblages, largely because the high grades associated with melting result in homogenisation of garnet, thus obliterating the prograde record. In this study we have exploited the presence of garnet crystals in migmatites that are of sufficient size to preserve evidence of prograde conditions in their cores. As a result we have traced the *P–T–t* evolution of a migmatite, recovered from the hanging wall of the Main Central Thrust (MCT) in the Sikkimese Himalaya, prior to, and during, melting, thus elucidating the thermal evolution of the MCT in the eastern Himalaya. Moreover, since the migmatite is from the High Himalayan Crystalline Series, a lithotectonic unit widely recognized as the source of the Miocene leucogranites of the Himalaya (Deniel *et al.*, 1987; Harris & Massey, 1994), this study

has generated the first direct measurement of the *P–T–t* path of an anatectic granite protolith.

GEOLOGICAL SETTING

The Main Central Thrust

Crustal thickening during the Himalayan orogeny is largely a result of thrust tectonics, with shortening being accommodated on a series of north-dipping thrust zones. The best-documented of these is the MCT (Heim & Gansser, 1939) that places the metasedimentary formations of the High Himalayan Crystalline Series (HHCS) onto the older, yet lower grade, metasediments of the Lesser Himalaya Formations (LHF). Estimates of shortening across the MCT range from 140 to 300 km (Lyon-Caen & Molnar, 1985; Schelling & Arita, 1991). The sparse quantitative constraints allow the interpretation that the displacement has increased eastwards along the strike of the MCT, possibly reflecting oblique collision between the Indian plate and Eurasia (Guillot *et al.*, 1999).

The MCT is not a single thrust marked by a discrete high-strain zone, but a wide zone (4–20 km thick) of distributed shear separating two sequences of metamorphosed sedimentary rocks (Jain & Manickavasagam, 1993) with an intermittent deformation history probably lasting over a period of at least 10 Myr (Harrison *et al.*, 1997). In Eastern Nepal a recent review of structures and chronology suggests that movement on the MCT by ductile shearing was initiated around 23 Ma and terminated at *c.* 16 Ma (Searle *et al.*, 2003). Sporadic reactivation at < 10 Ma, has been suggested from Pliocene monazite ages from the footwall of the MCT (Harrison *et al.*, 1997) but these have also been interpreted as progressive metamorphism in response to the insertion of thrust sheets within the Lesser Himalaya duplex (Robinson *et al.*, 2003). Geomorphic studies suggest the MCT remains active today (Hodges, 2000).

The *P–T–t* path of rocks affected by the MCT is particularly important since they may shed light on the causes of exhumation and of partial melting within the metasedimentary rocks of the High Himalaya. These formations are bounded by the MCT below and the South Tibetan detachment system (STDS) above. Melting within the sequence has been ascribed (i) to decompression, implying that melting will be coeval with decompression and that rock packages will be exhumed across their solidii (Harris & Massey, 1994), or (ii) to shear heating from movement along the MCT (Harrison *et al.*, 1998), in which case temperatures will be elevated close to the thrust zone at the time of movement (Royden, 1993). More recently, a thermomechanical model for the Himalayan orogen (Beaumont *et al.*, 2001) treats the HHCS as a low viscosity channel that has been extruded along the STDS and the MCT. Confirmation of partial melting at the MCT prior to exhumation would be consistent with channel flow within the HHCS since anatexis will severely reduce the viscosity of the material along the lower boundary of the proposed orogenic channel.

The MCT in Sikkim

The Eastern Himalaya, east of the Everest transect, have received scant attention relative to the more accessible valley transects to the west. The Sikkim–Darjeeling region lies in the western end of the Eastern Himalaya between 26 and 27 °N and 88–89 °E within the states of Sikkim and the northern part of West Bengal (Fig. 1). In Sikkim, the MCT is a ductile zone with strain distributed over several kilometres of apparently inverted metamorphism from garnet to sillimanite grade. The surface expression of the thrust delineates a loop, around which the Darjeeling migmatites and gneisses (HHCS) in the hanging wall are separated from the Daling schists, slates and quartzites (LHF) in the footwall by a narrow high-strain zone < 10 km wide of schists and orthogneisses (Gansser, 1964).

Most of what is known of metamorphism within the HHCS of Sikkim derives from studies north of Mangan (Fig. 1); for example, early work on this transect traces a narrow zone of schists and gneisses in the hanging wall of the MCT that increases rapidly in metamorphic grade from garnet-grade within the Daling schists up to sillimanite grade in the MCT zone, over a horizontal distance of 10–15 km (Mohan *et al.*, 1989). The muscovite-out isograd coincides with the northern boundary of the MCT zone. Garnet growth in both the Daling schists and the Darjeeling gneisses is generally syn-kinematic with top-to-the-south s-c fabrics (Mohan *et al.*, 1989, Neogi *et al.*, 1998). Movement on the thrust is poorly constrained in time but monazite growth ages from the MCT shear zone are interpreted as indicating movement at *c.* 22 Ma, 14–15 Ma and 12–10 Ma (Catlos *et al.*, 2003). Studies from the Bhutan transect, east of Sikkim, indicate that the MCT was active by 23 Ma (Daniel *et al.*, 2003).

P–T studies from the Darjeeling gneisses in Sikkim have concentrated on the upper part of the HHCS; these record a steep near-isothermal decompression path from 10 to 12 kbar at 800–850 °C to *c.* 5 kbar (Neogi *et al.*, 1998; Ganguly *et al.*, 2000). For samples closer to the MCT (< 10 km) conditions of *c.* 700 °C at 6–8 kbar have been deduced from garnet cores and *c.* 600 °C, *c.* 4.2 kbar from garnet rims (Neogi *et al.*, 1998), again suggesting decompression. A clockwise decompression path characterizes *P–T–t* evolution within the HHCS in other transects both to the east (Bhutan) and west (Everest) of Sikkim (Davidson *et al.*, 1997; Guillot *et al.*, 1999; Simpson *et al.*, 2000; Daniel *et al.*, 2003; Borghi *et al.*, 2003). The Kanchenjunga transect in eastern Nepal is an exception (Goscombe & Hand, 2000). Some confusion may

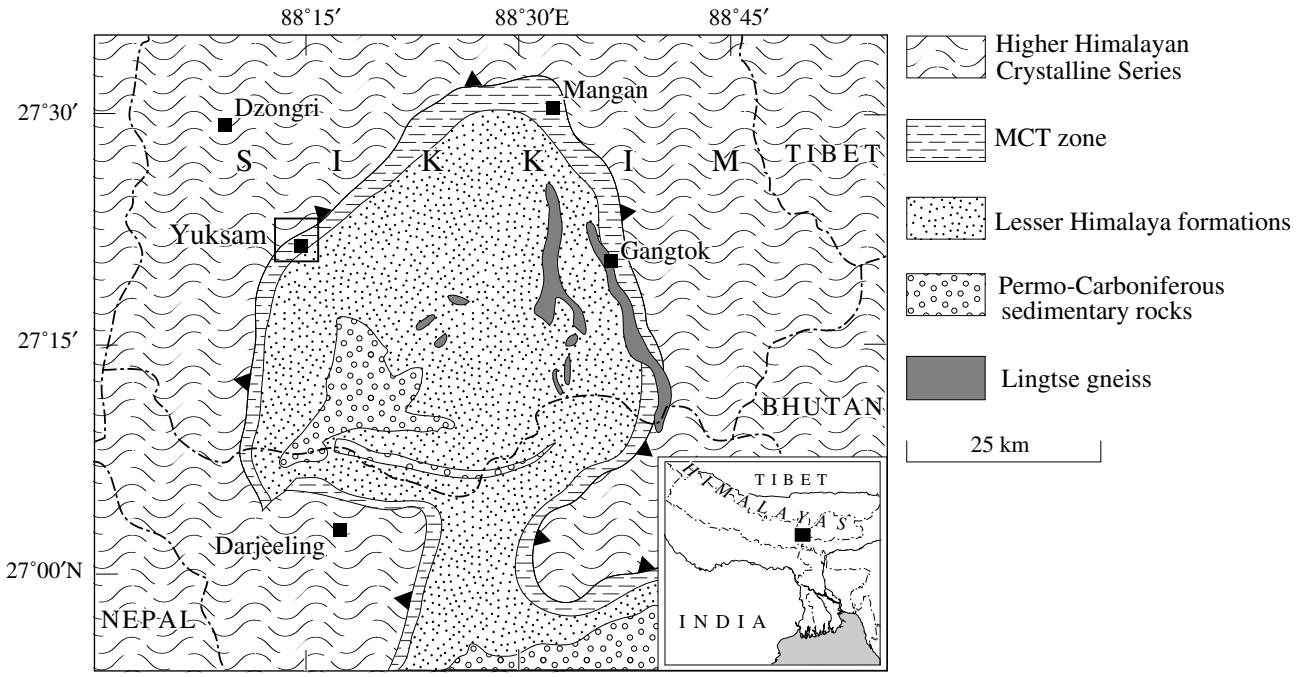

Fig. 1. Geological sketch map of the MCT zone from the Sikkim–Darjeeling region of the Eastern Himalaya (see inset for location). Box indicates location of Fig. 2.

result from the location of the MCT in this study, as commented on by Searle *et al*. (2003), in that the entire inverted metamorphic sequence is ascribed to the LHF rather than only the sub-kyanite grades.

The present study is an investigation of a sillimanite + kyanite-bearing migmatite from the Yuksam section, located 1.5 km NW of the MCT zone in the poorly known lower HHCS (SK14, Fig. 2). Given a regional dip of *c*. 45° NW, this is equivalent to a structural distance of *c*. 1 km above the MCT zone. Further north, a segregated garnet-tourmaline granite (SK12, Fig. 2) is located south of Bakhim, at a structural distance of about 2 km above the MCT zone. For many Himalayan transects in the central and western Himalaya, the hanging wall of the MCT comprises high-pressure (8–12 kbar), sub-solidus kyanite-bearing schists with melting occurring only up-section, coinciding with the sillimanite + alkali feldspar isograd (e.g. Inger & Harris, 1992; Vannay & Hodges, 1996). This observation has been cited as evidence that leucogranites are derived from the muscovite dehydration reaction during decompression (Harris & Massey, 1994). However, the presence of anatectic melts formed in the kyanite field would suggest that melt may have been present prior to decompression at pressures > 8–10 kbar (Le Breton & Thompson, 1988). Kyanite migmatites have also been noted in the hanging wall of the MCT in the Marsyandi transect of central Nepal (Coleman, 1998) and in eastern Bhutan (Daniel *et al*., 2003). The latter assemblages are cited as evidence for channel flow along the margins of the HHCS in the Bhutanese Himalaya (Grujic *et al*., 2002).

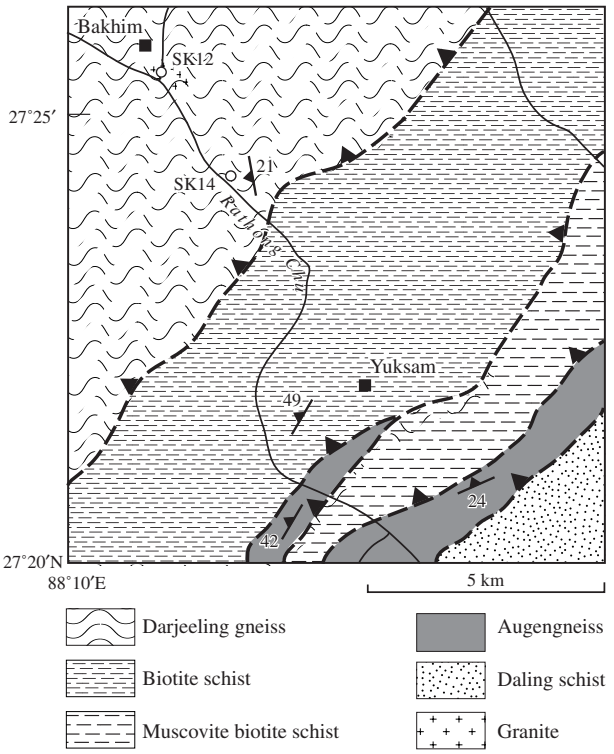

Fig. 2. Geological sketch map of the MCT region in the Yuksam transect, indicating the location of samples SK12 (27°25.483′ N, 88°11.348′ E) and SK14 (27°24.454′ N, 88°11.819′ E), within the Darjeeling gneisses of the HHCS. The MCT zone comprises pelitic schists and augengneiss, overthrust onto the Daling schists of the LHF.

Analytical techniques

Whole rock major and trace elements (Rb, Sr, Ba) were analysed on an ARL Fisons wavelength-dispersive XRF spectrometer at the Open University. Major elements were determined using glass discs prepared by fusing powdered samples with Spectroflux 105. Trace elements were determined from pressed powder pellets under run conditions described by Potts *et al.* (1984). REE were analysed using a VG PQ3 ICPMS instrument at Charles University in Prague. Rock powders were dissolved in HF-HNO3 mixture in screw-cap Savillex beakers over two days at 80 °C. The trace element concentrations were measured from 2% HNO3 solution using ^{115}In as an internal standard. Periodic checks of accuracy were carried out from measurements of international rock reference materials.

Mineral compositions were analysed using a Cameca SX50 electron microprobe fitted with an EDS Link system (i) at the Department of Earth Sciences, Cambridge University for melanosome assemblages and (ii) at the Department of Earth Sciences, Memorial University of Newfoundland, for leucosome assemblages using an accelerating voltage of 15–20 kV and a beam current between 3 and 20 nA. X-ray maps of garnet compositions were obtained from a Cameca SX100 microprobe at the Department of Earth Sciences, The Open University.

Garnet grains from several localities from the Yuksam transect were screened for inclusions, using SEM reconnaissance. All except one migmatite (SK14) were excluded from further study due to the presence of LREE-bearing accessory phases as inclusions. Garnet separates from the leucosome of SK14 were obtained by slicing and crushing garnet-rich portions of the rock and hand-picking under a binocular microscope to obtain an optically pure garnet separate of 20–50 mg. Samples were washed and transferred into PFA screw-cap beakers and spiked with a mixed ^{149}Sm/^{150}Nd spike. Chemical dissolution and separation techniques are described in Cohen *et al.* (1988) and Vance & O'Nions (1990). Nd concentrations and isotopic ratios of Nd were measured on a Micromass MC-ICPMS instrument (Isoprobe) at the Department of Geology, Royal Holloway College, University of London, using procedures described in Vance & Thirlwall (2002). The La Jolla Nd standard gave a value of ^{143}Nd/^{144}Nd = 0.511856 ± 13 during the period of analysis. Sm concentrations were determined by isotope dilution measurements using a VG 354 thermal ionisation mass spectrometer at Royal Holloway.

MIGMATITES IN SIKKIM

Petrography

The migmatites from above the MCT zone in the Yuksam transect are characterized by the assemblage quartz + alkali feldspar + plagioclase + biotite + garnet + kyanite + sillimanite. Lit-par-lit leucosomes form sub-horizontal garnet-bearing granite sheets, 5–50 mm wide (Fig. 3). In this study we consider the migmatites to comprise a leucosome (the granite sheets) and a melanosome (the biotite-rich gneisses); no genetic implications are attached to these terms. Such stromatic migmatites are common throughout the Darjeeling gneisses, but are particularly abundant in the section from the SK14 locality to about 10 km to the north-west at Dzongri.

Garnet is abundant throughout most pelitic rocks of the HHCS of Sikkim. In higher structural levels, zoned garnet comprises syn-tectonic, inclusion-rich cores and post-tectonic inclusion-free rims (Neogi *et al.*, 1998). In SK14, garnet is fairly abundant (2–8%); larger grains (2–5 mm), predominate in the leucosome with equant and subhedral habit (Fig. 4a,c). Melanosome garnet is anhedral and smaller (1–2 mm) often with embayed margins (Fig. 4b,d), particularly at the contact with sillimanite, suggesting a late period of garnet dissolution. Many garnet crystals contain inclusions of quartz, biotite, plagioclase, ilmenite and kyanite, particularly from within the melanosome.

The melanosome is an equigranular biotite–garnet gneiss with a mean grain size of 0.5–1.0 mm. The primary fabric of the melanosome is defined by biotite and by kyanite where it is surrounded by fibrolite, suggesting a polymorphic transformation of kyanite to sillimanite. Prismatic sillimanite (up to 4 mm long) is oriented parallel to foliation. Post-kinematic muscovite forms locally along the boundary with the leucosome, or mantling sillimanite. Rutile and ilmenite are accessory phases.

A coarser grainsize characterizes the leucosome (2–3 mm). Quartz (*c.* 20%) forms coarse interlocking crystals and is strain-free. Alkali feldspar (*c.* 50%) can be porphyroblastic (up to 8 mm across) and shows perthitic texture. Oligoclase (*c.* 20%) is unzoned and

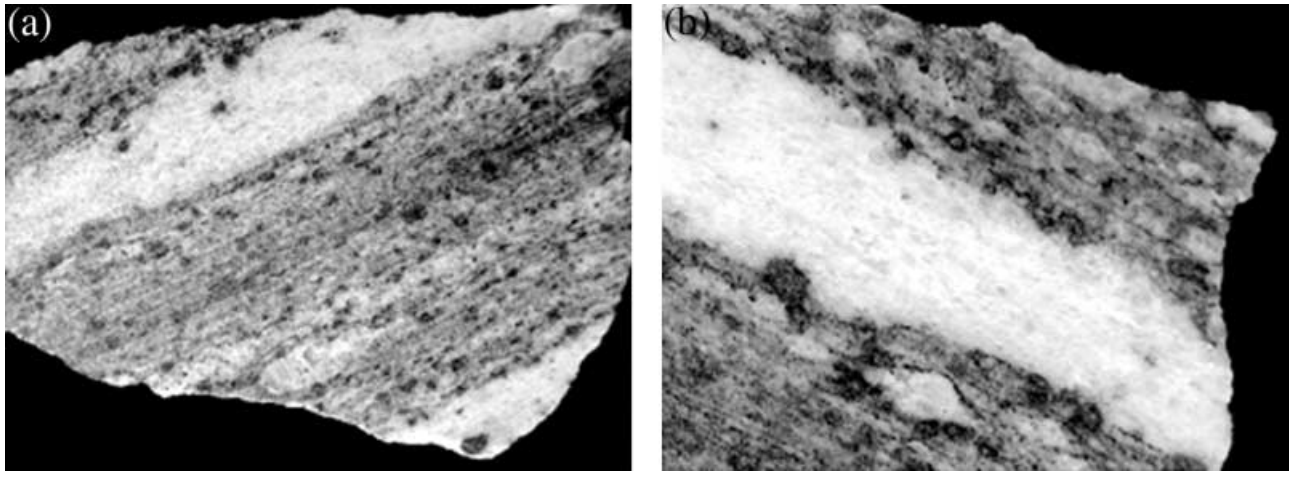

Fig. 3. Sectioned slab of stromatic migmatite SK14. Height of image (a) 10 cm; (b) 4 cm. Note large garnet within leucosome near boundary with melanosome.

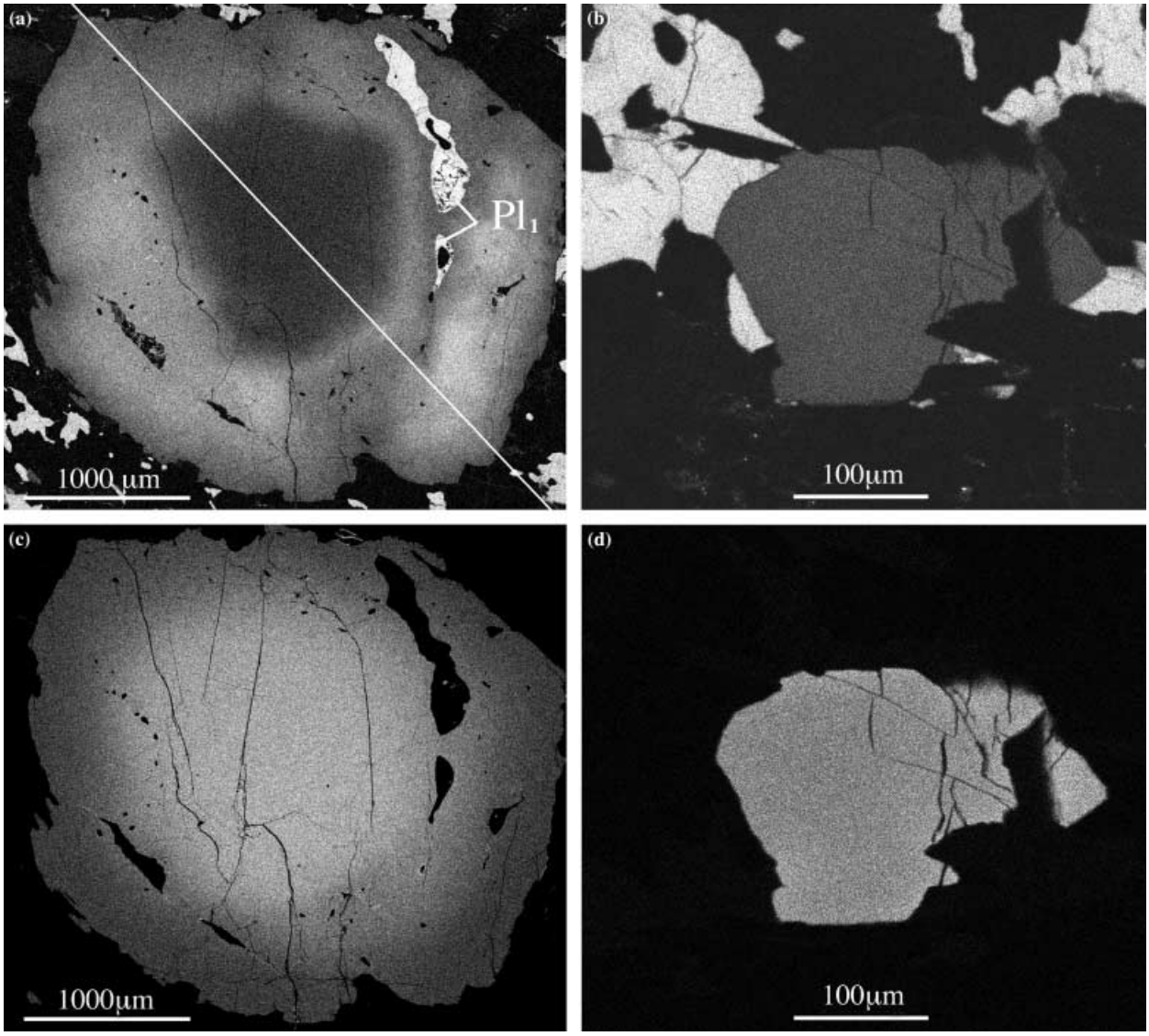

Fig. 4. X-ray maps showing compositional zoning patterns; for Ca (a) leucosome garnet Gl_1 (line indicates traverse of Fig. 5) (b) melanosome garnet (Gm); for Mn (c) leucosome garnet (Gl_1) (d) melanosome garnet (Gm). Gl_1 = 2 mm diameter, Gm = 0.2 mm diameter, Pl_1 indicates plagioclase inclusion in garnet.

displays albite twinning; myrmekite has developed along plagioclase/alkali feldspar grain boundaries. Within the leucosome, kyanite is restricted to inclusions within the cores of larger garnet. In contrast, both prismatic sillimanite and fibrolite are present in the matrix. The presence of sillimanite within the leucosomes in the absence of kyanite (except as inclusions to garnet) suggests that melting took place in the sillimanite stability field. Rutile and ilmenite form accessory phases.

There are some interesting comparisons between the Sikkimese migmatites described in this study and the kyanite-bearing migmatites from the Tashigang transect of eastern Bhutan (Davidson *et al*., 1997; Daniel *et al*., 2003) that appear in a similar structural position (*c*. 500 m above the MCT). Anatectic metasedimentary rocks from Bhutan comprise kyanite + garnet + two-mica migmatites with rare to abundant sillimanite. Kyanite varies in length from a few milimetres up to 5 cm, and is often deformed. As for the Sikkim migmatites, sillimanite is seen to replace kyanite which is consistent with decompression and/or heating into the sillimanite stability field. However the relative scarcity of sillimanite, and presence of kyanite within the matrix of the leucosome, led these authors to conclude that melting occurred within the kyanite stability field, prior to decompression. A second contrast is the strain-free textures of the leucosomes in the Yuksam transect compared with the strongly deformed nature of melt pods from eastern Bhutan (Daniel *et al*., 2003).

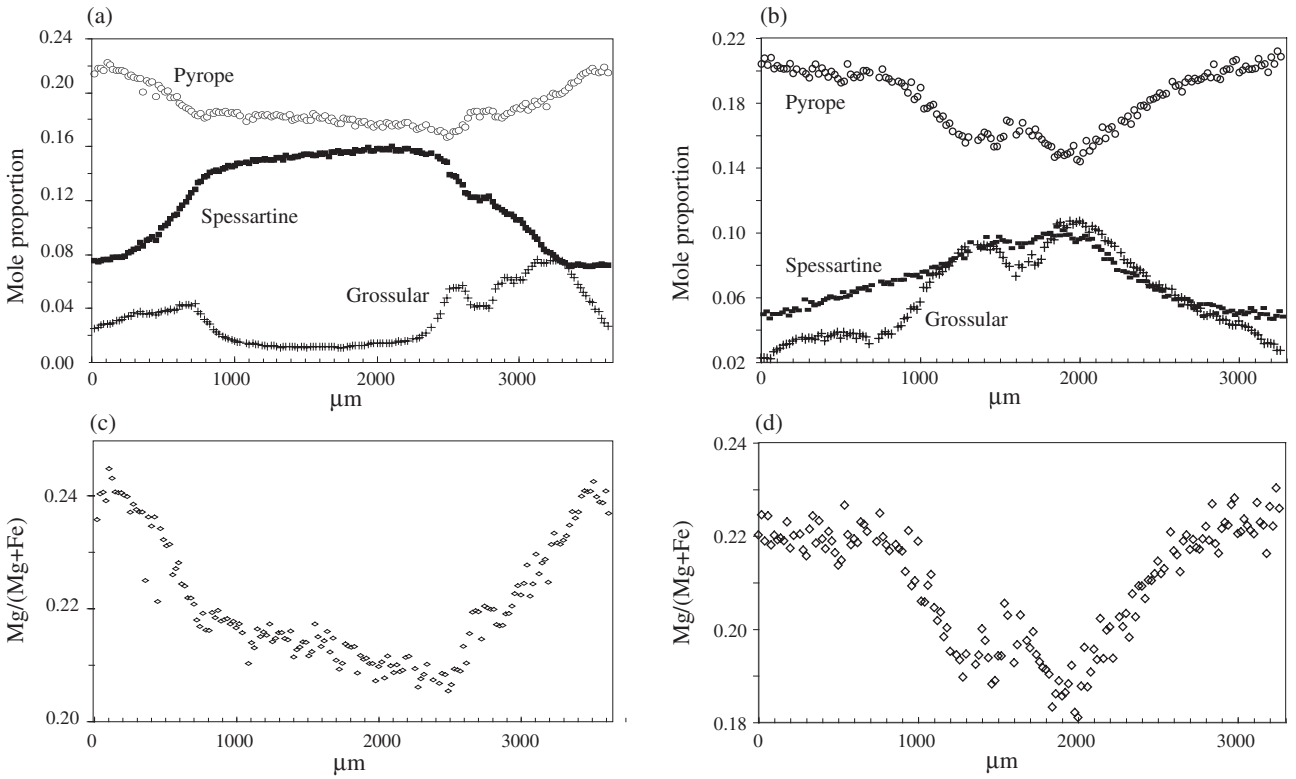

Fig. 5. Microprobe traverses of garnet from the leucosome; for pyrope, grossular and spessartine endmembers (a) for Gl_1 (b) for Gl_2; and Mg/(Mg + Fe) molar ratios (c) for Gl_1 (d) for Gl_2.

Mineral compositions

Two traverses across leucosome garnet (> 3 mm diameter) indicate contrasting compositional profiles. Gl_1 has spessartine-enriched cores (Fig. 5a) and a rimward increase in Mg/(Mg + Fe) (Fig. 5c), both indicative of prograde growth zonation (Tracy, 1982). The core is Ca-poor ($X_{grs} = 0.01$, Table 1), but X_{grs} rises sharply rimwards to 0.06 (Fig. 5a). The downward inflexion at 2.8 mm indicates post-entrapment changes in host chemistry around plagioclase inclusions (e.g. Whitney, 1991). Gl_2 also shows the rimward decrease in Mn and increase in Mg/(Mg + Fe) indicative of prograde zonation. However, the Gl_2 profile suggests a garnet core, within which there is an outward increase in grossular content from $X_{grs} = 0.08$ to $X_{grs} = 0.09$. Thus, within the centre of this core there is a minimum in grossular, but since this coincides with a maximum in Mg/(Mg + Fe) ratio and a minimum in spessartine, the inflexion does not reflect prograde growth, but rather is likely to be the result of coalescence between two smaller nucleii into one larger garnet grain early in the growth history. Across the mantle of Gl_2 (Fig. 5b), but not Gl_1 (Fig. 5a), there is strong zoning in Ca, decreasing rimward to $X_{grs} = 0.03$. For the same grain Mg/(Mg + Fe) increases from 0.18 (core) to 0.22 (rim).

Smaller garnet grains within the melanosome, have flat major-element profiles (Fig. 4b,d) suggesting that peak temperatures were sufficient to allow diffusional homogenisation. Some grains show rim zoning patterns indicative of retrograde re-equilibration.

Plagioclase grains in the leucosome are slightly zoned (Pl_2, $X_{an} = 0.19$–0.20) with albite-rich rims similar in composition to unzoned plagioclase in the melanosome (Pm, Table 1). Slightly more calcic plagioclase ($X_{an} = 0.23$) is preserved as inclusions within Gl_1 (Fig. 4a and Pl_1, Table 1). Biotite compositions are also fairly uniform; Mg/(Mg + Fe) ratios are lower in the melanosome than in the leucosome, as is also true for Mg/(Mg + Fe) ratios in garnet from the two domains, reflecting the differing bulk compositions. Biotite grains adjacent to, or included in, garnet have lower Mg/(Mg + Fe) ratios, due to retrograde diffusional exchange.

RESULTS

Geochemistry of the leucosome

The major-element composition of the leucosome is indicative of a highly peraluminous leucogranite (Table 2). Higher Rb/Sr ratios and lower Ba abundances in the leucosome compared to the melanosome are indicative of fluid-absent melting causing

Table 1. Representative microprobe analyses of SK14.

	Garnet									Biotite			Plagioclase					K Feldspar	
	leucosome							melanosome		leucosome		melanosome	leucosome			melanosome		leucosome	melanosome
	Gl_1(rim)	Gl_1(mantle)	Gl_1(core)	Gl_2(rim)	Gl_2(mantle)	Gl_2(out core)	Gl_2(in core)	Gm(core)	Gm(rim)	Bl_1	Bl_2	Bm	Pl_1(inc)	Pl_2(rim)	Pl_2(core)	Pm		Kl	Km
grain size (mm)	3.6	3.6	3.6	3.3	3.3	3.3	3.3	1	1	1	1	0.8	0.5	2	2	1		3	1
wt %																			
SiO_2	37.35	36.93	36.41	37.16	37.28	36.89	36.97	37.23	36.41	35.66	35.60	34.43	61.51	61.92	62.65	63.76		64.05	64.57
TiO_2	0.05	0.01	0.03	0.10	0.02	0.00	0.00	0.07	0.01	3.25	3.56	3.61	0.00	0.00	0.11	0.24		0.28	
Al_2O_3	21.60	21.51	21.37	21.97	22.02	21.71	21.42	21.14	21.16	18.52	18.21	17.84	23.23	23.35	23.08	23.34		18.50	19.40
Fe_2O_3	1.89	2.60	3.05	1.14	1.45	1.38	1.72	1.74	2.05										
FeO	28.37	27.45	27.60	31.93	31.20	28.33	28.59	33.65	34.06	16.69	17.49	19.23	0.13	0.00	0.00	0.00		0.00	0.00
MnO	3.94	5.97	7.02	2.24	2.71	4.34	4.41	1.62	1.93	0.06	0.02	0.00	0.03	0.00	0.00	0.00		0.00	0.00
MgO	4.99	4.53	4.51	5.22	5.13	3.67	4.21	4.39	3.57	10.15	10.08	8.75	0.00	0.00	0.00	0.14		0.00	0.02
CaO	2.66	2.03	0.39	0.80	1.19	3.79	2.85	1.14	0.91	0.00	0.08	0.00	4.84	3.99	4.23	4.13		0.00	0.08
Na_2O	0.00	0.00	0.00	0.00	0.00	0.00	0.00	0.00	0.00	0.11	0.26	0.23	8.79	9.45	9.34	8.96		1.80	1.39
K_2O	0.02	0.00	0.10	0.00	0.00	0.00	0.00	0.00	0.00	9.67	9.67	9.76	0.35	0.20	0.17	0.37		14.30	14.98
Total	100.87	101.04	100.49	100.57	101.00	100.12	100.18	100.98	100.10	94.10	94.97	93.85	98.88	99.02	99.48	100.81		98.91	100.72
Cations	12 Ox	12 Ox	12 Ox	12 Ox	12 Ox	12 Ox	12 Ox	12 Ox	12 Ox	11 Ox	11 Ox	11 Ox	8 Ox	8 Ox	8 Ox	8 Ox		8 Ox	8 Ox
Si	2.94	2.92	2.91	2.94	2.93	2.94	2.94	2.96	2.93	2.72	2.70	2.68	2.76	2.77	2.79	2.80		2.98	2.95
Ti	0.00	0.00	0.00	0.01	0.00	0.00	0.00	0.00	0.00	0.19	0.20	0.21	0.00	0.00	0.00	0.00		0.01	0.01
Al	2.00	2.01	2.01	2.05	2.04	2.04	2.01	1.98	2.01	1.66	1.63	1.64	1.23	1.23	1.21	1.21		1.01	1.05
Fe^{3+}	0.11	0.16	0.18	0.07	0.09	0.08	0.10	0.10	0.12										
Fe^{2+}	1.87	1.82	1.84	2.11	2.05	1.89	1.90	2.23	2.29	1.06	1.11	1.25	0.00	0.00	0.00	0.00		0.00	0.00
Mn	0.26	0.40	0.48	0.15	0.18	0.29	0.30	0.11	0.13	0.00	0.00	0.00	0.00	0.00	0.00	0.00		0.00	0.00
Mg	0.59	0.53	0.54	0.62	0.60	0.44	0.50	0.52	0.43	1.15	1.14	1.01	0.00	0.00	0.00	0.01		0.00	0.00
Ca	0.22	0.17	0.03	0.07	0.10	0.32	0.24	0.10	0.08	0.00	0.01	0.00	0.23	0.19	0.20	0.19		0.00	0.00
Na	0.00	0.00	0.00	0.00	0.00	0.00	0.00	0.00	0.00	0.02	0.04	0.04	0.77	0.82	0.81	0.76		0.16	0.12
K	0.00	0.00	0.00	0.00	0.00	0.00	0.00	0.00	0.00	0.94	0.94	0.97	0.02	0.01	0.01	0.02		0.85	0.88
Endmember concentrations																			
pyp	0.20	0.18	0.19	0.21	0.21	0.15	0.17	0.18	0.15	phl	0.52	0.51	0.45	an	0.23	0.19	0.20	0.20	san	0.84	0.88
grs	0.08	0.06	0.01	0.02	0.03	0.11	0.08	0.03	0.03	ann	0.48	0.49	0.55	ab	0.77	0.81	0.80	0.80	ab	0.16	0.12
alm	0.64	0.62	0.64	0.72	0.70	0.64	0.65	0.76	0.78										
sps	0.09	0.14	0.16	0.05	0.06	0.10	0.10	0.04	0.05										
Endmember activities																			
pyp	0.012	0.009	0.008	0.012	0.011	0.006	0.008	0.007	0.004	phl	0.051	0.047	0.034	an	0.32	0.26	0.28	0.28	san	0.85	0.88
grs	0.0008	0.00034	0.000003	0.000024	0.000075	0.002	0.00092	0.000057	0.000029	ann	0.035	0.039	0.057	ab	0.76	0.81	0.80	0.78			
alm	0.23	0.21	0.23	0.34	0.31	0.24	0.24	0.4	0.44	east	0.047	0.042	0.033								
sps	0.0006	0.0022	0.0037	0.00012	0.0002	0.00084	0.00089	0.00004	0.00008										

Mineral abbreviations after Kretz (1983).

Table 2. Bulk composition of granite (SK12) and migmatite (SK14).

	SK12	SK14 Leucosome	SK14 Melanosome
wt %			
SiO_2	75.84	75.03	70.89
TiO_2	0.03	0.04	0.74
Al_2O_3	14.70	14.51	14.31
Fe_2O_3	0.14	0.10	0.73
FeO*	0.19	0.22	4.83
MnO	0.02	0.02	0.13
MgO	0.49	0.08	1.53
CaO	0.38	0.62	1.01
Na_2O	3.79	2.57	2.16
K_2O	3.04	6.37	3.34
P_2O_5	0.21	0.09	0.10
LOI	0.42	0.30	0.33
Total	99.30	99.95	100.11
p.p.m.			
Rb	111	280	235
Sr	2	132	165
Ba	33	356	684
La	0.8	28.4	53.1
Ce	1.7	43.2	80.4
Pr	0.3	5.7	10.8
Nd	1.1	19.8	38.8
Sm	0.6	4.1	7.3
Eu	0.02	0.75	1.48
Gd	0.32	2.69	4.82
Tb	0.07	0.46	0.75
Dy	0.30	2.78	4.64
Ho	0.04	0.58	1.00
Er	0.08	1.47	2.58
Tm	0.02	0.23	0.44
Yb	0.10	1.41	2.75
Lu	0.02	0.21	0.42
Mode (vol %)†			
Qtz	40	21	53
Pl	32	23	5
Kfs	19	49	11
Bt	2	0	19
Grt	2	1	3
Sil/Ky	2	6	8
Ms	0	0	1

* Ferrous/ferric ratios by titration.
† Determined by point-counting (2000 points).

low melt fractions and peritectic alkali feldspar (Harris *et al.*, 1995). The major-element chemistry is, in many respects, similar to that of the segregated granite from the same section (SK12, Table 2), excepting K_2O abundances that are much higher in the leucosome. However, the chemistry of the leucosome should not be taken as indicative of a melt that has formed and crystallized in a closed system. This is because migmatite leucosomes may incorporate not only crystallized melt, but also peritectic phases, and possibly cumulate minerals from an extracted melt (Sawyer, 1987; Ellis & Obata, 1992; Otamendi & Patiño Douce, 2001). In the case of SK14, the modal abundances of both alkali feldspar and aluminosilicate are in excess of values from a crystallized melt and confirm their incorporation, probably as peritectic products of the melt reaction. The temperature of the melt, as deduced from monazite dissolution and LREE saturation curves, is 748 °C (from the calibration of Montel, 1993); this provides a minimum constraint on the solidus temperature since the coexistence of peritectic phases and crystallized melt in the leucosome would yield lower apparent solidus temperatures than would be obtained from a pure melt, assuming such phases contain negligible REE abundances.

Sm–Nd dating

Bulk rock values for the whole rock sample of SK14 yielded $\varepsilon_{Nd} = -13$ (Table 3), with a model Nd age of 1600 Ma, values typical of HHCS sedimentary rocks from across the Himalaya (Ahmad *et al.*, 2000) and of the Miocene leucogranites derived from them (Harris & Massey, 1994). The ages obtained from the garnet fractions, extracted from the leucosome adjacent to the melanosome boundary, relative to the bulk rock Sm–Nd composition are 16.1 ± 2.4 Ma and 23.0 ± 2.6 Ma for rim and core, respectively (Fig. 6). Nd concentrations of the garnet separate vary from 0.6 to 1.1 p.p.m., well within the range obtained from *in situ* Nd analysis of garnet (Schwandt *et al.*, 1996) and so consistent with the interpretation that measured Sm and Nd abundances originate from the garnet lattice rather than from sub-microscopic inclusions of LREE-enriched accessory phases. This inference is supported by the observation that the older garnet (Gs2) has lower REE abundances which precludes the older age being determined by the presence of pre-garnet accessory phases.

Depending on the diffusivity of Nd in garnet, garnet ages may reflect the time of either growth or of cooling through a closure temperature. The closure temperature of Nd in garnet is controversial and appears to be a function not only of grain size and cooling rate but also of the starting temperature from which it cools (Ganguly *et al.*, 1998a). For a 3 mm

Table 3. Sm-Nd isotopic data of garnet and whole rock from sample SK14.

		[Sm] (p.p.m.)	± 2σ	[Nd] (p.p.m.)	± 2σ	$^{147}Sm/^{144}Nd$	± 2σ	$^{143}Nd/^{144}Nd$	± 2σ	ε_{Nd}
WR	whole rock	3.9074	0.0031	19.1107	0.0056	0.1236	0.0001	0.511985	0.000014	−13
										Age (Ma)*
Gs1	garnet rim	2.3887	0.0039	1.1071	0.0002	1.3043	0.0021	0.512110	0.000012	16.1 ± 2.4
Gs2	garnet core	1.2432	0.0024	0.5842	0.0002	1.2864	0.0025	0.512160	0.000016	23.0 ± 2.8

* Age of garnet using the whole rock as the low Sm/Nd phase. Errors (2σ) are based upon propagation of analytical uncertainties.

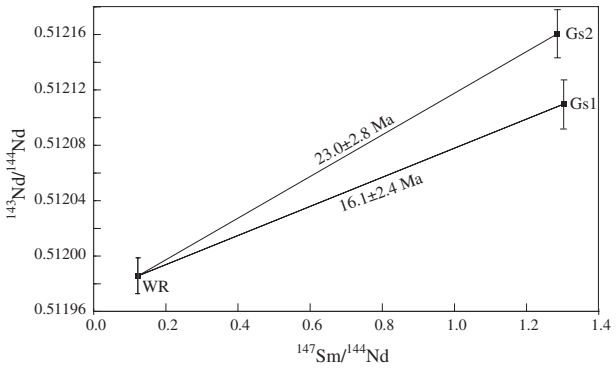

Fig. 6. Sm–Nd isotope data for whole rock (WR) and two garnet separates (Gs1, Gs2) from the leucosome of SK14. Uncertainties (2σ) are based on propagation of analytical uncertainties.

grain, cooling at 25 °C Myr^{-1} from an initial temperature of 750 °C, similar to peak temperatures deduced from this study, experimental constraints and diffusion modelling indicate that the closure temperature would be *c*. 710 °C (Ganguly *et al*., 1998a). However, given the uncertainties in this estimate and the preservation of major-element prograde zonation (Fig. 5) it is probable that the garnet ages from SK14 are either growth ages, or reflect cooling ages within the uncertainties of the time of garnet growth. Both ages are therefore robust and indicate either the time of garnet growth, or the mean age of several periods of growth.

It is concluded therefore that the garnet was growing from, or before, 23 ± 3 Ma. The older age may date peak metamorphic grade in the kyanite field prior to melting. It coincides with early movement on the MCT, as determined from monazite from the MCT zone in Sikkim (Catlos *et al*., 2003) and from the Bhutan transect (Daniel *et al*., 2003). We see no sign of prograde Oligocene metamorphism (*c*. 32 Ma) as recorded in accessory phases from the top of the HHCS in the Everest transect (Simpson *et al*., 2000; Searle *et al*., 2003). However, we cannot rule out the possibility that the core ages are an average age for garnet growth between *c*. 30 and *c*. 18 Ma.

The younger age (16 ± 2 Ma) lies within the uncertainties of U–Pb ages from kyanite migmatites above the MCT in Bhutan (18–14 Ma; Daniel *et al*., 2003) and of the age of monazite growth from the LHF near the MCT in Sikkim at 15–14 Ma (Catlos *et al*., 2003). It is the youngest age obtained so far from direct dating of a Himalayan garnet.

P–T conditions of garnet growth

In order to assign tectonic significance to the chronological constraints, the *P–T* evolution of the rock needs to be established. The first-order conclusion from the observed textures is that garnet growth occurred within the kyanite field and that the rock subsequently entered the sillimanite field where melting took place. The presence of sillimanite needles within the leucosome, and absence of primary muscovite in the melanosome, suggest that dehydration melting of muscovite occurred within the sillimanite stability field by the reaction:

$$\text{muscovite} + \text{plagioclase} + \text{quartz} = Al_2SiO_5 + \text{K-feldspar} + \text{melt} \quad (1)$$

The preservation of growth zoning patterns in the larger garnet crystals suggests a short residence time at high temperatures. Applying appropriate diffusion coefficients (Ganguly *et al*., 1998b), the preservation of Rayleigh growth profiles for Mn in large grains (2–3 mm, Fig. 5b) and the homogenisation of compositions in smaller grains (< 1 mm, Fig. 4d) suggests that temperatures > 750 °C could only have been maintained for 0.5–2 Myr. At a prograde heating rate of 15–25 °C Myr^{-1} (Vance & Harris, 1999) this suggests a maximum subsequent temperature of *c*. 800 °C, followed by rapid cooling.

The garnet core of Gl_1 (Fig. 5a) provides the highest Mn contents observed from garnet in SK14, although yet higher values may be present if the grain has not been sectioned through its core. Since Mn is strongly partitioned into garnet, garnet growth depletes the chemical reservoir from which it grows in Mn. Hence the Gl_1 garnet core is a sample of a garnet that formed early in the history of the migmatite. Across about 1 mm of this core, both Mn and Ca display flat compositional profiles (Fig. 5a). For Mn, this flattening may be due to diffusional homogenisation. Diffusivities are somewhat lower for Ca than for Mn and the relative timescales of Ca homogenisation is about 20% longer for Ca within 1 mm garnet at 750 °C (Chakraborty & Ganguly, 1992). Studies of grossular abundances in coexisting garnet of various sizes indicate that compositional heterogeneities during crystal growth may be preserved under amphibolite facies conditions (Chernoff & Carlson, 1997, 1999). However, such variations are relatively minor (e.g. CaO varying from 0.8 to 1.3 wt% in Fig. 3 of Chernoff & Carlson, 1997) compared to the order-of-magnitude contrast in CaO observed between the cores of Gl_1 and Gl_2. In pelitic assemblages, equilibration of Ca between garnet and plagioclase is achieved by a net transfer reaction, rather than diffusive exchange. Since the core of Gl_1 (diameter *c*. 1 mm) is much smaller than that of Gl_2 (> 2 mm) it may be argued that low-Ca garnet, preserved as smaller cores in SK14, result from re-equilibration at low pressures. Only in the larger cores (e.g. Gl_2) are prograde conditions preserved.

The mantle surrounding the low-Ca garnet core (Gl_1) records a sharp increase in Ca, and plagioclase included in this outer part of the garnet (Pl_1(inc), Table 1) is more calcic than that from the matrix. Both observations are consistent with the garnet mantle

growing in equilibrium with a melt. Garnet growth within the melt field above the muscovite melting reaction results from

$$\text{biotite} + \text{plagioclase} + \text{quartz} + Al_2SiO_5 = \text{garnet} \pm \text{K-feldspar} + \text{melt} \quad (2)$$

The garnet will be enriched in grossular relative to the sub-solidus phase as it equilibrates with the residual plagioclase that is anorthite-rich relative to the sub-solidus plagioclase (Spear & Kohn, 1996; Whitehouse & Platt, 2003). Pl_1(inc) is therefore a refractory plagioclase formed during melting.

In contrast, the rimward decrease in X_{grs} from the outer core of Gl_2 is interpreted as indicating growth during substantial decompression. For this garnet, the mantle shows a flat profile for X_{grs} at *c*. 0.034 mole proportion (Fig. 5b), reflecting growth during melting following decompression.

To elucidate the quantitative *P–T* history of the migmatite, pressure-temperature pseudosections were drawn in the system Na_2O-CaO-MnO-K_2O-FeO-Fe_2O_3-MgO-Al_2O_3-TiO_2-SiO_2-H_2O (NaCaMnKFMASHTO), using the method of Powell *et al*. (1998), version 3.1 of the program THERMOCALC (Powell & Holland, 2001) and an updated version of the Holland & Powell (1998) dataset. Activity-composition relationships of phases were modified from Holland & Powell (1998), White *et al*. (2000) and White *et al*. (2001), with the addition of Mn end-members to garnet, biotite, chlorite, staurolite and cordierite (as in Mahar *et al*., 1997). Margules parameters for all Mn-bearing couples were set at zero with the exception of $W_{pyp,sps} = 4.5$ (e.g. Wood *et al*., 1994). The eight end-member melt model of Powell & Holland (2001) was utilised.

For an inhomogeneous rock, such as a migmatite, it is necessary to identify the bulk composition from which the observed phases have formed. If the leucosome in sample SK14 resulted from *in situ* melting of a homogeneous protolith, then the composition of that protolith may be obtained by combining melanosome and leucosome compositions in the appropriate proportions; at outcrop scale the relative proportions are approximately 60% melanosome, 40% leucosome. The lack of evident melt-escape networks suggests that closed-system conditions prevailed during anatexis, such that a mixed melanosome + leucosome bulk composition is an appropriate approximation of the pre-melting bulk composition. Any significant deviation from closed system behaviour during the *P–T* loop, as would result for example from melt injection, would alter the subsequent composition resulting in increased uncertainties in each pseudosection. This effect is difficult to quantify, but the available evidence (in terms of macro-textures and the apparent consistency between the mixed-composition pseudosection and observed assemblages) suggests that cation loss or infiltration was limited. Hence Fig. 7 illustrates the inferred assemblage for a rock of composition equivalent to 60% melanosome and 40% leucosome from SK14, as determined from bulk analyses (Table 2).

The stability field of biotite is particularly sensitive to oxygen fugacity during metamorphism. Low-to-moderate oxidation levels were assumed from the lack of visible hematite and magnetite in either melanosome or leucosome and from titration chemistry on the bulk samples (Table 2) and were set as in White *et al*. (2000).

A key prediction of this phase diagram (Fig. 7) is that upon heating to the wet solidus (labelled 'A' on inset), small fraction melts will form but will be volumetrically buffered as water is instantaneously dissolved into the melt phase. Although grain boundary melts will be achieved in such a way, at pressures above *c*. 3.2 kbar a maximum melt fraction, *F*, of 0.05–0.1 cannot be exceeded without heating to the muscovite breakdown reaction (labelled 'B' on inset). An additional 3–5 °C of heating across this K-feldspar forming reaction will result in an increase in *F* from *c*. 0.1 to *c*. 0.3, with $F > 0.4$ achieved at temperatures in the range 750–800 °C for pressures of 4–8 kbar, in agreement with results experimentally determined from Himalayan pelitic schists (Patiño Douce & Harris, 1998). At temperatures above the muscovite-out reaction, *F* will be enhanced by the garnet-forming reaction (2). To avoid confusion, pseudosection fields are labelled here as either 'liq', implying a significant melt fraction ($F > 0.1$) or '(liq)' (note parentheses) for grain boundary melts ($F < 0.1$).

Pre-melt conditions

It has been argued above that prograde conditions are best preserved in the larger garnet cores, such as from Gl_2. Within the field Grt-Pl-Ky-Ms, the Ca isopleth for the outer core of this garnet ($X^{Ca}_{Grt} = 0.11$) indicates pressures of 9–11 kbar (Fig. 7). However, a degree of disequilibrium for Ca can be preserved during prograde conditions (Chernoff & Carlson, 1997, 1999) which can introduce significant errors in the application of Ca isopleths in pseudosections constructed from bulk chemistry compositions to the interpretation of individual garnet cores.

An alternative approach is to obtain the pressure from garnet core and coexisting plagioclase, using the reaction

$$\text{grossular} + Al_2SiO_5 + \text{quartz} = \text{anorthite}. \quad (3)$$

Temperature estimates lie in the range 670–770 °C (as evidenced by the presence of kyanite and lack of melt in garnet inclusions). Using Gl_2 core and matrix plagioclase compositions, a pressure of 11 ± 1 to 13 ± 1 kbar is obtained from reaction (3) as calculated from Powell & Holland (1994) with end-member activities provided by the program AX (available for download from T. Holland at http://www.esc.cam.ac.uk/astaff/holland/ax.html). This is strictly a minimum constraint since early growth of high-pressure, grossular-rich garnet will

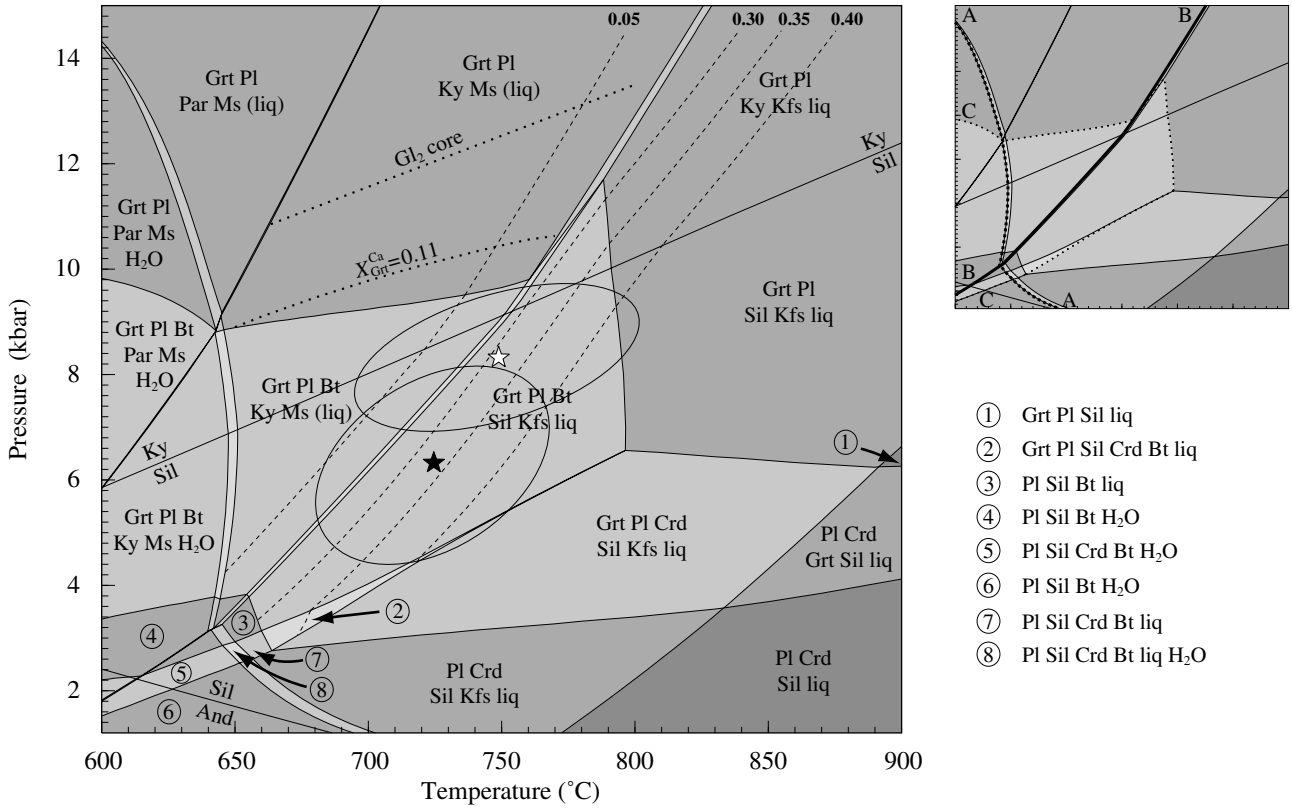

Fig. 7. NaCaMnKFMASHTO pseudosection with quartz and ilmenite in excess for mixed leucosome + melanosome compositions (SK14). Mineral abbreviations as in Kretz (1983). The white star represents leucosome peak conditions as determined by THERMOCALC's average *PT* mode and compositions of the mantle of garnet Gl_2 and matrix phases with $a_{H_2O} = 0.6$ (ellipse is 1σ uncertainty). The black star represents melanosome peak conditions of garnet Gm and matrix phases. The dashed lines are contours of equal melt fraction *F*, and are labelled in the top right corner. The dotted lines represent equilibrium for Gl_2 core formation (see text for details) and a X^{Ca}_{Grt} pseudosection isopleth. Inset highlights three key stabilities; A = wet solidus, B = muscovite melting reaction, C = limit of biotite stability.

coexist with plagioclase with a slightly lower anorthite activity than that which equilibrates at lower pressures with the garnet rim. For the melanosome assemblage > 90% of the total Ca budget resides in plagioclase compared with < 10% in garnet. This means that the Ca partitioning between plagioclase and garnet is buffered by the anorthite component such that the plagioclase composition was almost invariant during garnet growth. Mass balance constraints indicate that the composition of plagioclase coexisting with the grossular-rich garnet core lies between An_{20} (the present plagioclase composition in the melanosome) and An_{18} (assuming 90% of the Ca budget resides in plagioclase). The less anorthite-rich composition would increase the calculated pressure by < 0.4 kbar. Hence the estimates of peak pressures calculated by two distinct methods lie within an uncertainty of ± 1 kbar.

Conditions during melting

Kyanite is absent as a matrix phase in the leucosome and is partially replaced in the melanosome by prismatic and fibrolitic sillimanite, indicating that melting occurred at lower pressure. To obtain average *P–T* estimates from coexisting assemblages an estimate of H_2O activity is required. This has been estimated by minimising σ_{fit} (the statistical scatter in the residuals as defined in Powell & Holland, 1994) to give a value of $a_{H_2O} = 0.6$. Assuming H_2O activities of 0.6, THERMOCALC average *PT* calculations yield peak temperatures of 749 ± 49 °C at 8.3 ± 1.5 kbar (based on the Gl_2-mantle composition) or 725 ± 50 °C at 6.3 ± 1.7 kbar (from Gm-rim), implying a period of pre-anatexis decompression. The pseudosection shown in Fig. 7 demonstrates that simple decompression of SK14 from *c.* 11 to *c.* 7 kbar (even without a concomitant temperature increase) would result in significant melt generation, at which point separate pseudosections for the leucosome (representing the melt and peritectic phases) and melanosome (the unmelted domain) become appropriate. It should be stressed that these two pseudosections represent end-member cases for conditions that prevailed during melting.

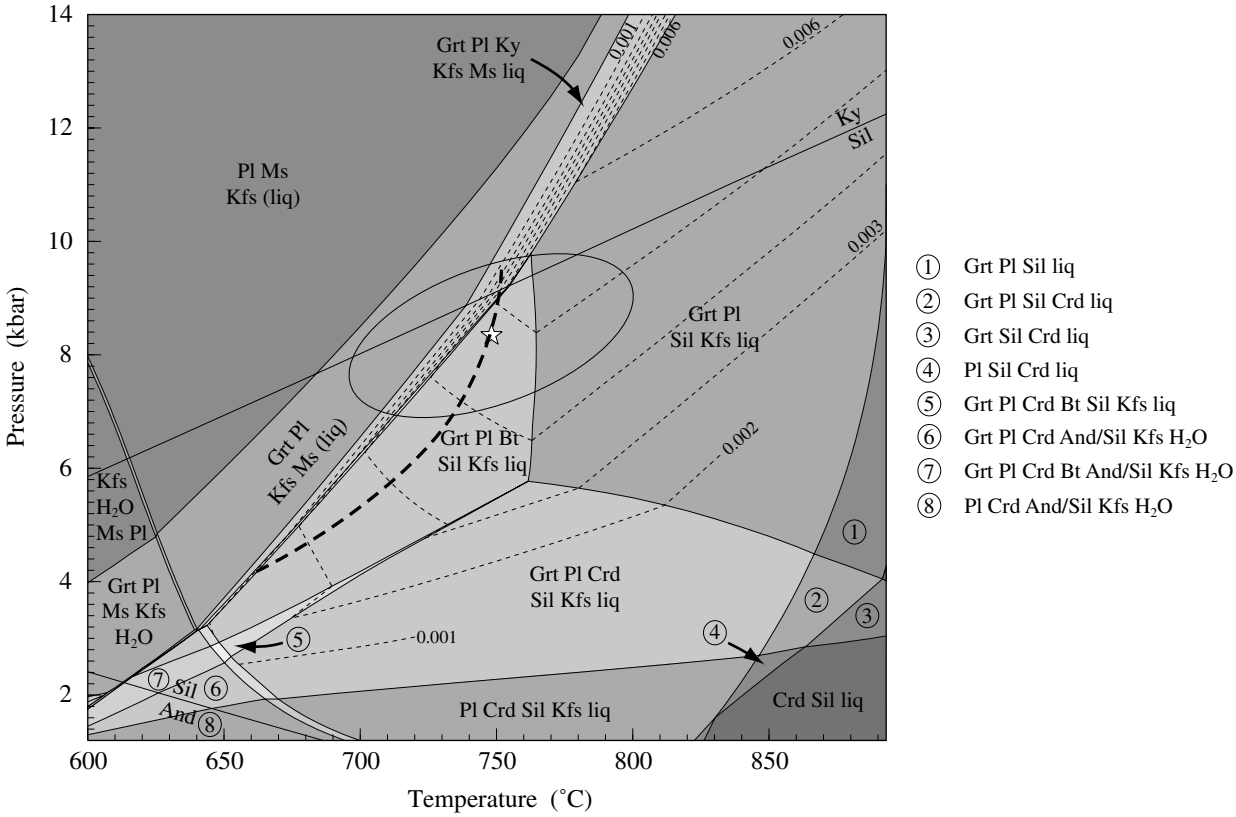

Fig. 8. NaCaMnKFMASHTO pseudosection with quartz and ilmenite in excess for leucosome compositions (SK14). The white star and ellipse represents peak conditions as described in Fig. 7. Dashed lines represent predictions of modal proportion of garnet in selected fields. Bold dashed curve is segment of *P–T* loop constrained by this diagram.

Leucosome evolution

The leucosome pseudosection (Fig. 8) is contoured for modal proportion garnet, showing that muscovite-dehydration melting is accompanied by a significant growth of garnet, as evidenced by the large euhedral mantle of crystal Gl_2. As decompression continues, the modal proportion of garnet decreases, resulting in partial resorption provided the exhumation rate is slow enough for reaction kinetics to keep pace.

As the melt re-crystallizes at temperatures of 660–680 °C, at 4.0–4.4 kbar, significant K-feldspar, plagioclase feldspar (and quartz) crystallization will occur. As this proceeds, H_2O will begin to be exsolved and will either be expelled or will back-react with K-feldspar to form muscovite. In SK14 it appears that exsolved H_2O was expelled and reacted to form muscovite mats at the margins of the segregations. The lack of biotite in the leucosome is consistent with biotite breakdown on cooling at *c.* 660 °C and 4.2 kbar although even if the exhumation rate was too rapid for the retrograde reaction to occur, the pseudosection predicts that the assemblage would contain only trace abundances of biotite ($< 1\%$).

Melanosome evolution

The melanosome pseudosection (Fig. 9) is of particular significance in estimating the minimum pressure that was reached during the high-temperature decompression phase, because of the absence of cordierite in the rock and its presence at low pressures on the pseudosection. This indicates a minimum pressure of 4–5 kbar at temperatures of 700–730 °C, with the threshold decreasing to *c.* 2.8–3.0 kbar below the wet solidus. Similarly, the maximum pressure of the retrograde stage of the loop can be constrained by the lack of staurolite in the assemblage. For temperatures of 600 °C, the absence of staurolite signifies pressures below *c.* 4.6 kbar, although it could be argued that the absence of staurolite growth at lower temperatures may result from sluggish nucleation rates.

Modal garnet contouring of the melanosome pseudosection also suggests garnet growth as the muscovite-out melt reaction is crossed, but at a more modest rate compared with the leucosome (the mode increases from *c.* 0.115 to *c.* 0.125 as compared with < 0.001 to *c.* 0.006 in the leucosome). This would result in comparatively more garnet in the melanosome than in leucosome, but with a higher proportion of the leucosome garnet formed at high temperature in the presence

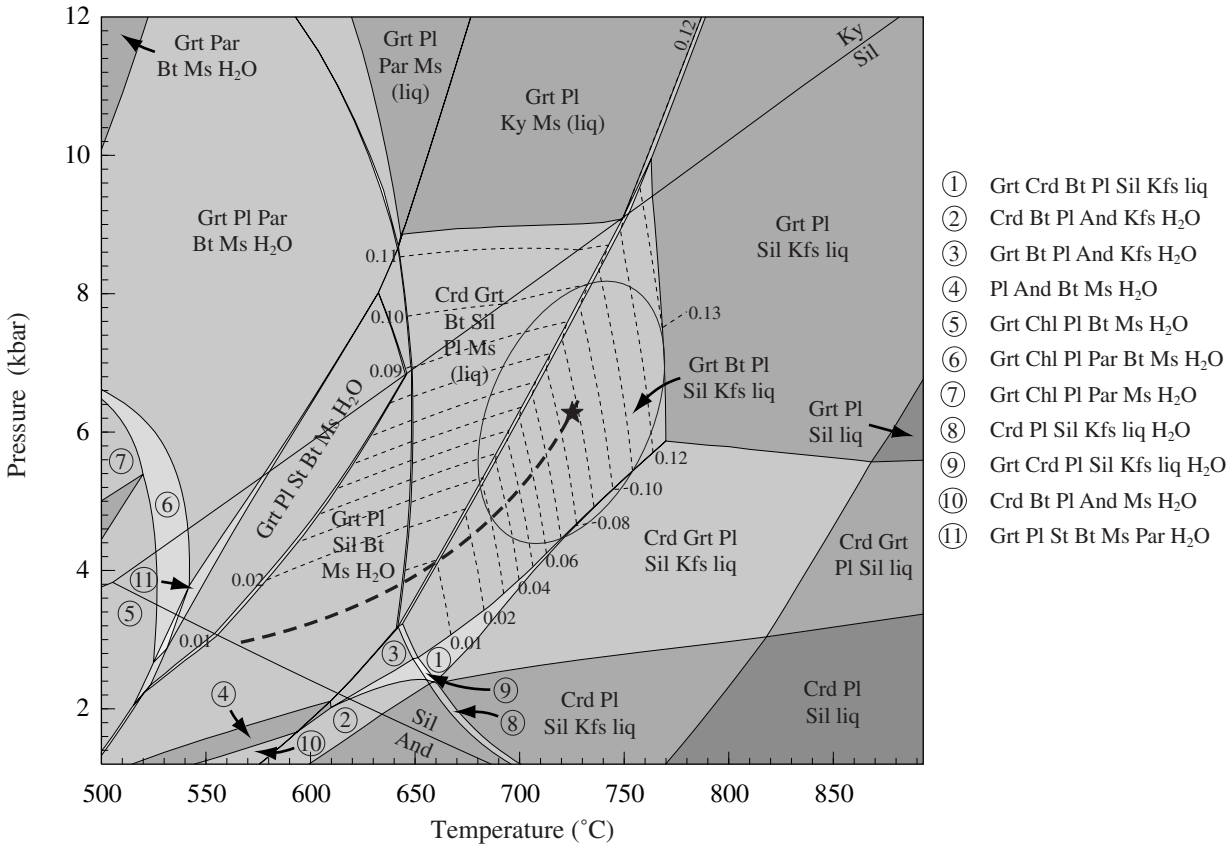

Fig. 9. NaCaMnKFMASHTO pseudosection with quartz and ilmenite in excess for melanosome compositions (SK14). The black star and ellipse represents peak conditions as described in Fig. 7. Dashed lines represent predictions of modal proportion of garnet in selected fields. Bold dashed curve is segment of *P–T* loop constrained by this diagram.

of melt. In reality, these are end-member cases because the original bulk composition was actively un-mixing to form leuco- and melanosomes during this time. However, it does suggest that large euhedrally mantled garnet porphyroblasts (such as crystal Gl_2) grew as a result of crystal position, requiring an inherited core and a zone undergoing muscovite-dehydration driven anatexis. Texturally, the interface between melt and restite might prove an ideal site for such mineral growth, as is apparent in Fig. 3, whilst areas without a supply of melt (such as a depleted melanocratic zone or muscovite deficient regions) will experience significantly less garnet growth.

During the first 100 °C of cooling from the postulated peak, the modal proportion of garnet in the melanosome declines from > 0.11 to < 0.02, explaining the significant degree of resorption that must have occurred to form such ragged crystals as are seen in the melanosome (Fig. 4). The sub-solidus *P–T* path will not result in significant modification of the garnet mode until lower temperature (below *c*. 550 °C).

DISCUSSION

Combining information from all three pseudosections we conclude that the migmatite underwent decompression from about 11 to 7 kbar. This indicates *c*. 12 km of exhumation over a period of 6.9 ± 3.7 Ma determined from the garnet isotopic data, indicating a rate of 2 ± 1 mm yr^{-1} which compares with 2–3 mm yr^{-1} cited for the HHCS in the Everest region from Ar cooling ages (Searle *et al*., 2003) and with *c*. 4 mm yr^{-1} for the top of the HHCS in Sikkim, deduced from numerical modelling of compositional zoning of garnet in metapelites (Ganguly *et al*., 2000).

In order to determine the geometry of the *P–T–t* path during exhumation from the mid-crust at the rate inferred from this study, we have applied a simple 1D thermal model to a crust that doubled in thickness at 45 Ma, assuming the thermal parameters of England *et al*. (1992). A rock at a depth of 37 km (11.5 kbar) will have reached 740 °C by 23 Ma, from internal heating of the thickened crust. If it is then exhumed at a rate of 2 mm yr^{-1}, the computed path reaches a peak of *c*. 765 °C at 17 Ma (Fig. 10). In reality the latent heat of melting will moderate this modest temperature increase so that decompression becomes effectively isothermal. By 13 Ma the *P–T–t* path cools rapidly due to heat loss to the surface. Although the model is generalised and incorporates many uncertainties, the relative rates of internal heating and exhumation

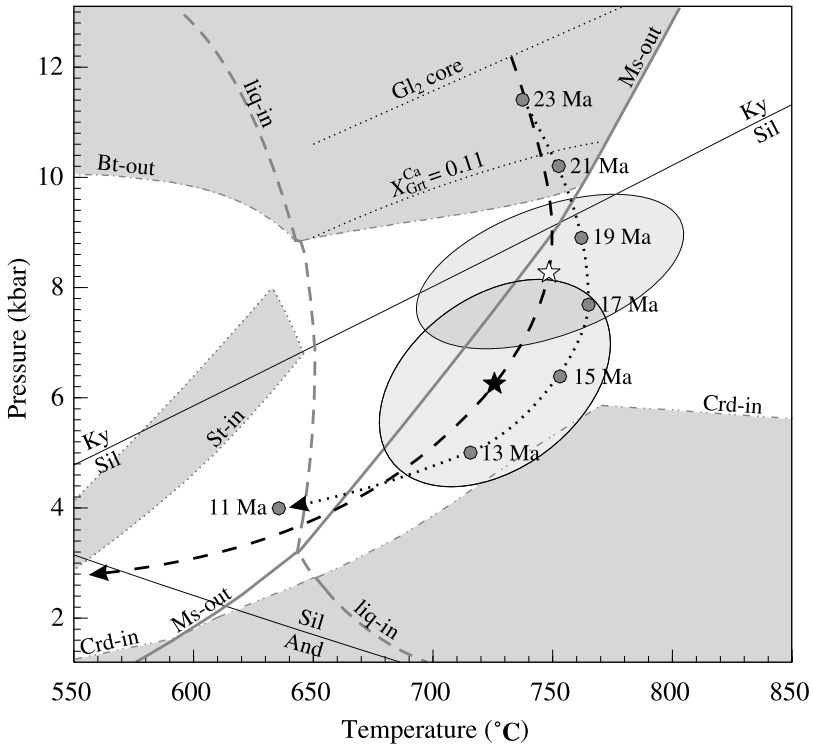

Fig. 10. Proposed *P–T* evolution of SK14 determined from pseudosections and numerical modelling. The bold dashed curve represents an evolutionary path as constrained by Figs 7–9. The bold dotted curve is derived from a 1D thermal model for uplift of sample from a pressure of 11 kbar at 23 Ma, at a constant exhumation rate of 2 mm yr^{-1}; dots indicate time in Ma (see text for discussion). Wet melting curve, muscovite-out and biotite-out reactions, uncertainty ellipses, X_{Grt}^{Ca} isopleth and Gl_2 core equilibrium, as given in Fig. 7. Staurolite and cordierite stabilities as in Fig. 9.

suggest an effectively isothermal *P–T–t* path during exhumation through the mid crust, followed by rapid cooling from depths of *c*. 6 kbar. This is consistent with both the *P–T* and the geochronological constraints obtained in this study. The results also imply that at distances of *c*. 1 km from the MCT zone, neither dissipative heating along the thrust, nor advective cooling from the underthrust slab, are required to model realistic *P–T–t* paths during exhumation.

The results from this study suggest that, at least for the Yuksam section of Sikkim, decompression of *c*. 4 kbar caused melting well within the sillimanite field (Figs 7 & 8). Given the absence of notable mafic selvedges (Fig. 3), it is likely that the melt sites were determined by pre-existing compositional variations. Specifically, melting would be initiated along grain boundaries in assemblages where the reactants, muscovite, plagioclase and quartz coexisted in proportions close to those of the 'optimum mode' (Patiño Douce & Johnston, 1991).

An important question is how typical are these findings for the MCT assemblages elsewhere in the Eastern Himalaya? Specifically, was anatexis in the hanging wall of the MCT in the eastern Himalaya earlier than, or a consequence of, decompression? The kyanite-bearing migmatites immediately above the MCT in Bhutan are inferred to have cooled from peak temperatures during the underthrusting of the cooler Lesser Himalayan rocks and then experienced decompression to pressures of 5 kbar (Davidson *et al*., 1997; Daniel *et al*., 2003). This sequence of prograde melting, cooling and finally decompression is deduced from the scarcity of sillimanite associated with the leucosomes. However, these observations allow an alternative explanation that reconciles their findings with the present study. For compositions similar to SK14, decompression at temperatures above *c*. 770 °C will result in melting within the kyanite field (Fig. 7), suggesting perhaps that the Bhutanese migmatites were exhumed from a slightly greater depth, or at a slightly younger time, and so were at marginally higher temperatures during decompression. In other words, a minor elevation in starting temperature would allow the interpretation that the Bhutanese migmatites also melted after decompression. The period of decompression deduced from the Sikkim migmatite (23–16 Ma) coincides with the period of granite melt generation in the eastern Himalaya (Schärer, 1984; Simpson *et al*., 2000; Searle *et al*., 2003). Interestingly, east of the Yadong cross-structure somewhat younger crustal melts (18–13 Ma) are recorded in Bhutan and southern Tibet (Edwards & Harrison, 1997; Daniel *et al*., 2003), consistent with an eastward younging of tectonic events.

From studies in the Everest transect, the early movement on the MCT has been constrained to *c*. 20 Ma, coeval with movement on the STDS (Searle *et al*., 2003). This compares with findings from the MCT in Bhutan that conclude the thrust was active by 23 Ma (Daniel *et al*., 2003). From monazite work in Sikkim (Catlos *et al*., 2003) the MCT movements seem to have been intermittent until about 10 Ma. In southern Tibet to the north of Bhutan, melting and STDS movement occurred at < 12.5 Ma (Edwards &

Harrison, 1997). Taken together the evidence suggests that both the STDS and the MCT were intermittently active in the eastern Himalaya from *c*. 23 to *c*. 10 Ma, providing the mechanism for extrusion of the HHCS. The cause of extrusion has been ascribed to either channel flow (Grujic *et al*., 2002) or exhumation of a tectonic wedge (Harris & Massey, 1994) during the Late Miocene. This study can not resolve this uncertainty, but the evidence from garnet zoning profiles from the hanging wall of the MCT in Sikkim is that melting followed exhumation. This would be consistent with melting being either caused by, or enhanced by, decompression, rather than *vice versa*.

ACKNOWLEDGEMENTS

We thank T. Holland for invaluable advice during the construction of the pseudosections. Field work (NBWH) was supported by a Royal Society Research Grant. JK was supported by GACR project no. 205/01/1112. MC and SG were supported by studentships funded by NERC and the Nehru Trust, respectively. We are grateful to D. Waters and C. Daniel for perceptive and constructive reviews.

REFERENCES

Ahmad, T., Harris, N., Bickle, M., Chapman, H., Bunbury, J. & Prince, C., 2000. Isotopic constraints on the structural relationships between the Lesser Himalayan Series and the High Himalayan Crystalline Series, Garhwal Himalaya. *Geological Society of America Bulletin*, **112,** 467–477.

Beaumont, C., Jamieson, R. A., Nguyen, M. H. & Lee, B., 2001. Himalayan tectonics explained by extrusion of a low-viscosity crustal channel coupled to focused surface denudation. *Nature*, **414,** 738–742.

Borghi, A., Castelli, D., Lombardo, B. & Visonà, D., 2003. Thermal and baric evolution of garnet granulites from the Kharta region of S Tibet, E Himalaya. *European Journal of Mineralogy*, **15,** 401–418.

Catlos, E. J., Harrison, T. M. & Dubey, C. S., 2003. MCT duplex formation in the Sikkim Himalaya. *18th Himalaya-Karakoram-Tibet Workshop, Ascona, Switzerland, Abstract volume*, 29.

Chakraborty, C. & Ganguly, J., 1992. Cation diffusion in aluminosilicate garnets; experimental determination in spessartine-almandine diffusion couples, evaluation of effective binary, diffusion coefficients, and applications. *Contributions to Mineralogy and Petrology*, **111,** 74–86.

Chernoff, C. B. & Carlson, W. D., 1997. Disequilibrium for Ca during growth of pelitic garnet. *Journal of Metamorphic Geology*, **15,** 421–438.

Chernoff, C. B. & Carlson, W. D., 1999. Trace element zoning as a record of chemical disequilibrium during garnet growth. *Geology*, **27,** 555–558.

Cohen, A. S., O'Nions, R. K., Siegentheler, R. & Griffin, W. L., 1988. Chronology of the pressure-temperature history recorded by a granulite terrain. *Contributions to Mineralogy and Petrology*, **98,** 303–311.

Coleman, M. E., 1998. U-Pb constraints on Oligocene-Miocene deformation and anatexis within the Central Himalaya, Marsyandi Valley, Nepal. *American Journal of Science*, **298,** 553–571.

Daniel, C. G., Hollister, L. S., Parrish, R. R. & Grujic, D., 2003. Exhumation of the Main Central Thrust from lower crustal depths, Eastern Bhutan Himalaya. *Journal of Metamorphic Geology*, **21,** 317–334.

Davidson, C., Grujic, D. E., Hollister, L. S. & Schmid, S. M., 1997. Metamorphic reactions related to decompression and synkinematic intrusion of leucogranite, High Himalayan Crystallines, Bhutan. *Journal of Metamorphic Geology*, **15,** 593–612.

Deniel, C., Vidal, P., Fernandez, A., Le Fort, P. & Peucat, J. J., 1987. Isotopic study of the Manaslu granite (Himalaya, Nepal): Inferences of the age and source of Himalayan leucogranites. *Contributions to Mineralogy and Petrology*, **96,** 78–92.

Edwards, M. A. & Harrison, T. M., 1997. When did the roof collapse? Late Miocene north–south extension in the High Himalaya revealed by Th-Pb monazite dating of the Khula Kangri granite. *Geology*, **25,** 543–546.

Ellis, D. J. & Obata, M., 1992. Migmatite and melt segregation at Cooma, New South Wales. *Transactions of the Royal Society of Edinburgh, Earth Sciences*, **83,** 95–106.

England, P., Le Fort, P., Molnar, P. & Pêcher, A., 1992. Heat sources for Tertiary magmatism and anatexis in the Annapurna-Manaslu region of Central Nepal. *Journal of Geophysical Research*, **97,** 2107–2128.

Foster, G., Vance, D., Kinny, P., Prince, C. & Harris, N., 2000. The significance of monazite U-Th-Pb age data in metamorphic assemblages; a combined chemical and isotopic study. *Goldschmidt Conference Abstracts*, Volume 5, p. 405. Cambridge Publications.

Foster, G., Vance, D., Harris, N. & Argles, T., 2002. The Tertiary collision-related thermal history and tectonic evolution of the NW Himalaya. *Journal of Metamorphic Geology*, **20,** 827–844.

Ganguly, J., Cheng, W. & Chakraborty, S., 1998b. Cation diffusion in aluminosilicate garnets: experimental determination in pyrope-almandine diffusion couples. *Contributions to Mineralogy and Petrology*, **131,** 171–180.

Ganguly, J., Dasgupta, S., Cheng, W. & Neogi, A., 2000. Exhumation history of a section of the Sikkim Himalayas, India: records in the metamorphic mineral equilibria and compositional zoning of garnet. *Earth and Planetary Science Letters*, **183,** 471–486.

Ganguly, J., Tirone, M. & Hervig, R. L., 1998a. Diffusion kinetics of samarium and neodymium in garnet, and a method for determining cooling rates of rocks. *Science*, **281,** 805–807.

Gansser, A., 1964. *Geology of the Himalaya*. John Wiley & Sons, London.

Goscombe, B. & Hand, M., 2000. Contrasting *P-T* paths in the Eastern Himalaya, Nepal: inverted isograds in a paired metamorphic belt. *Journal of Petrology*, **41,** 1673–1719.

Grujic, D., Hollister, L. S. & Parrish, R. R., 2002. Himalayan metamorphic sequence as an orogenic channel: insight from Bhutan. *Earth and Planetary Science Letters*, **198,** 177–191.

Guillot, S., Cosca, M., Allemand, P. & Le Fort, P., 1999. Contrasting metamorphic and geochronologic evolution along the Himalayan belt. *Geological Society of America, Special Paper*, **328,** 117–128.

Harris, N., Ayres, M. & Massey, J., 1995. The geochemistry of granitic melts produced during the incongruent melting of muscovite: implications for the extraction of Himalayan leucogranite magmas. *Journal of Geophysical Research*, **100,** 15767–15777.

Harris, N. B. W. & Massey, J. A., 1994. Decompression and anatexis of Himalayan metapelites. *Tectonics*, **13,** 1537–1546.

Harrison, T. M., Grove, M., Lovera, O. M. & Catlos, E. J., 1998. A model for the origin of Himalayan anatexis and inverted metamorphism. *Journal of Geophysical Research*, **103,** 27017–27032.

Harrison, T. M., Ryerson, F. J., Le Fort, P., Yin, A., Lovera, O. M. & Catlos, E. J., 1997. A Late Miocene-Pliocene origin for the Central Himalayan inverted metamorphism. *Earth and Planetary Science Letters*, **146,** E1–E7.

Heim, A. & Gansser, A., 1939. Central Himalaya. Geological observations of the Swiss expedition, 1939. *Denkschriften der Schweizerischen Naturforschenden Gesellschaft*, **73,** 1–245.

Hodges, K. V., 2000. Tectonics of the Himalayan and southern Tibet from two perspectives. *Geological Society of America Bulletin*, **112,** 324–350.

Holland, T. J. B. & Powell, R., 1998. An internally consistent thermodynamic data set for phases of petrological interest. *Journal of Metamorphic Geology*, **16,** 309–343.

Inger, S. & Harris, N. B. W., 1992. Tectonothermal evolution of the High Himalayan Crystalline Sequence, Langtang Valley, northern Nepal. *Journal of Metamorphic Geology*, **10,** 439–452.

Jain, A. K. & Manickavasagam, R. M., 1993. Inverted metamorphism in the intracontinental ductile shear zone during Himalayan collision tectonics. *Geology*, **21,** 407–410.

Kretz, R., 1983. Symbols for rock-forming minerals. *American Mineralogist*, **68,** 277–279.

Le Breton, N. & Thompson, A. B., 1988. Fluid-absent (dehydration) melting of biotite in metapelites in the early stages of crustal anatexis. *Contributions to Mineralogy and Petrology*, **99,** 226–237.

Lyon-Caen, H. & Molnar, P., 1985. Gravity anomalies, flexure of the Indian plate and the structure, support and evolution of the Himalaya and the Ganga Basin. *Tectonics*, **4,** 513–538.

Mahar, E., Powell, R., Holland, T. J. B. & Howell, N., 1997. The effect of Mn on mineral stability in metapelites. *Journal of Metamorphic Geology*, **15,** 223–238.

Mohan, A., Windley, B. F. & Searle, M. P., 1989. Geothermobarometry and development of inverted metamorphism in the Darjeeling-Sikkim region of the eastern Himalaya. *Journal of Metamorphic Geology*, **7,** 95–110.

Montel, J. M., 1993. A model for monazite/melt equilibrium and application to the generation of granitic magmas. *Chemical Geology*, **110,** 127–146.

Neogi, S., Dasgupta, S. & Fukuoka, M., 1998. High *P-T* polymetamorphism, dehydration melting, and generation of migmatites and granites in the Higher Himalayan Crystalline Complex, Sikkim, India. *Journal of Petrology*, **39,** 61–99.

Otamendi, J. E. & Patiño Douce, A. E., 2001. Partial melting of aluminous metagreywackes in the Northern Sierra de Comechingones. *Journal of Petrology*, **42,** 1571–1772.

Patiño Douce, A. E. & Harris, N., 1998. Experimental constraints on Himalayan anatexis. *Journal of Petrology*, **39,** 689–710.

Patiño Douce, A. E. & Johnston, A. D., 1991. Phase equilibria and melt productivity in the pelitic system: implications for the origin of peraluminous granitoids and aluminous granulites. *Contributions to Mineralogy and Petrology*, **107,** 202–218.

Potts, P. J., Webb, P. C. & Watson, J. S., 1984. Energy dispersive X-ray fluorescence analysis of silicate rocks for major and trace elements. *X-Ray Spectrometry*, **13,** 2–15.

Powell, R. & Holland, T. J. B., 1994. Optimal geothermometry and geobarometry. *American Mineralogist*, **79,** 120–133.

Powell, R. & Holland, T. J. B., 2001. Course Notes for the THERMOCALC Workshop 2001, Virginia: 'Calculating Metamorphic Phase Equilibria'. CD-ROM.

Powell, R., Holland, T. J. B. & Worley, B., 1998. Calculating phase diagrams involving solid solutions via non-linear equations, with examples using THERMOCALC. *Journal of Metamorphic Geology*, **16,** 577–588.

Robinson, D. M., DeCelles, P. G., Garzione, C. N., Pearson, O. N., Harrison, T. M. & Catlos, E. J., 2003. Kinematic model for the Main Central thrust in Nepal. *Geology*, **31,** 359–362.

Royden, L. H., 1993. The steady state thermal structure of eroding orogenic belts and accretionary prisms. *Journal of Geophysical Research*, **98,** 4487–4507.

Sawyer, E. W., 1987. The role of partial melting and fractional crystallization in determining discordant migmatite leucosome compositions. *Journal of Petrology*, **28,** 445–473.

Schärer, U., 1984. The effect of initial ^{230}Th disequilibrium on young U-Pb ages: the Makalu, Himalaya. *Earth and Planetary Science Letters*, **67,** 191–204.

Schelling, D. & Arita, K., 1991. Thrust tectonics, crustal shortening and the structure of the far-eastern Nepal Himalaya. *Tectonics*, **10,** 851–862.

Schwandt, C. S., Papike, J. J. & Shearer, C. K., 1996. Trace element zoning in pelitic garnet of the Black Hills, South Dakota. *American Mineralogist*, **81,** 1196–1207.

Searle, M. P., Simpson, R. L., Law, R. D., Parrish, R. R. & Waters, D. J., 2003. The structural geometry, metamorphic and magmatic evolution of the Everest massif, High Himalaya of Nepal. *Journal of the Geological Society of London*, **160,** 345–366.

Simpson, R. L., Parrish, R. R., Searle, M. P. & Waters, D. J., 2000. Two episodes of monazite crystallisation during metamorphism and crustal melting in the Everest region of the Nepalese Himalaya. *Geology*, **28,** 403–406.

Spear, F. S. & Kohn, M. J., 1996. Trace element zoning in garnet as a monitor of crustal melting. *Geology*, **24,** 1099–1102.

Tracy, R. J., 1982. Compositional zoning and inclusions in metamorphic minerals. In: *Characterisation of Metamorphism Through Mineral Equilibria, Reviews in Mineralogy* (ed. Ferry, J. M.), pp. 355–397. Mineralogical Society of America, Washington.

Vance, D. & Harris, N. B. W., 1999. The timing of early decompression in the Himalaya: implications for crustal melting. *Geology*, **27,** 395–398.

Vance, D. & O'Nions, R. K., 1990. Isotopic chronometry of zoned garnets: growth kinetics and metamorphic histories. *Earth and Planetary Science Letters*, **97,** 227–240.

Vance, D. & Thirlwall, M., 2002. An assessment of mass discrimination in MC-ICPMS using Nd isotopes. *Chemical Geology*, **185,** 227–240.

Vannay, J. C. & Hodges, K. V., 1996. Tectonothermal evolution of the Himalayan metamorphic core between the Annapurna and Dhaulagiri, central Nepal. *Journal of Metamorphic Geology*, **14,** 635–656.

White, R. W., Powell, R. & Holland, T. J. B., 2001. Calculation of partial melting equilibria in the system Na_2O-CaO-K_2O-FeO-MgO-Al_2O_3-SiO_2-H_2O (NCKFMASH). *Journal of Metamorphic Geology*, **19,** 139–153.

White, R. W., Powell, R., Holland, T. J. B. & Worley, B., 2000. The effect of TiO_2 and Fe_2O_3 on metapelitic assemblages at greenschist and amphibolite facies conditions: mineral equilibria calculations in the system K_2O-FeO-MgO-Al_2O_3-SiO_2-H_2O-TiO_2-Fe_2O_3. *Journal of Metamorphic Geology*, **18,** 497–511.

Whitehouse, M. J. & Platt, J. P., 2003. Dating high-grade metamorphism – constraints from rare-earth elements in zircon and garnet. *Contributions to Mineralogy and Petrology*, **145,** 61–74.

Whitney, D. L., 1991. Calcium depletion halos and Fe-Mn-Mg zoning around faceted plagioclase inclusions in garnet from a high-grade pelitic gneiss. *American Mineralogist*, **76,** 493–500.

Wood, B. J., Hackler, R. T. & Dobson, D. P., 1994. Experimental determination of Mn-Mg mixing properties in garnet, olivine and oxide. *Contributions to Mineralogy and Petrology*, **115,** 438–448.

Received 29 August 2003; revision accepted 21 January 2004.